Mechanistic Insights into CO and H_2 Oxidation on Cu/CeO_2 Single Atom Catalysts: A Computational Investigation

Parinya (Lewis) Tangpakonsab[1], Alexander Genest[1]*, Gareth S. Parkinson[2], Günther Rupprechter[1]

[1]Institute of Materials Chemistry, TU Wien, Getreidemarkt 9/BC, A-1060 Vienna, Austria
[2]Institute of Applied Physics, TU Wien, Wiedner Hauptstrasse 8-10/134, 1040 Vienna, Austria

Abstract

Single atom catalysts (SACs) have attracted significant interest due to their unique properties and potential for enhancing catalytic performance in various chemical reactions. In this study, we atomistically explore adsorption properties and catalytic performance of single Cu atoms anchored at low-index Cu/CeO_2 surfaces, focusing on the oxidation of CO and H_2. Utilizing density functional theory (DFT) calculations, we report that Cu adatoms bind favorably on different Cu/CeO_2 surfaces, following a stability order of (100)>(110)>(111). The charge transfer from a single adsorbed Cu atom to Ce leads to the reduction of Ce^{4+} to Ce^{3+} and the oxidation of Cu^0 to Cu^+. This strengthens molecular bonds at Cu sites, particularly for CO, while H_2 shows a by ∼1 eV weaker adsorption. CO oxidation is energetically more favorable than H_2 oxidation on the $Cu/CeO_2(111)$ surface. The rate-controlling steps for the Mars-van Krevelen oxidation involve the formation of a bent CO_2^- intermediate for CO and H_2O for H_2. The lattice oxygen atom at the interface plays a key role for both oxidation processes. Our findings highlight the potential of single atom catalyst, Cu/CeO_2, for CO adsorption and oxidation in heterogeneous catalysis.

Keywords— Single atom catalysis, Cu, CeO_2, CO oxidation, H_2 oxidation, DFT

1 Introduction

Transition metal (TM) oxides are of great importance for various applications, including, energy generation and storage, [1–5] gas sensing, [6–10] and heterogeneous catalysis. [11–18] Among these, CeO_2 (ceria) has been extensively studied as a support material in heterogeneous catalysis due to its remarkable redox properties, which are beneficial for oxygen storage/release and the transport of excess electrons into Ce(4f) states. [19–26] The use of ceria as a support for metal nanoclusters and nanoparticles, such as gold [27–32] and copper, [11, 33–35] has been studied both experimentally and theoretically. Gold and copper particles supported on ceria have been frequently applied for (low temperature) CO oxidation [11, 28, 35–38] as well as CO preferential oxidation (CO-PROX) under hydrogen-rich conditions, [11,39] and water-gas shift reactions. [20,29,40,41] In all cases the catalytic activity is related to the high redox ability of the ceria support.

When metals like Au or Cu engage in interfaces with ceria, electron transfer occurs from the metal atoms to the Ce atoms of the ceria surface. [42] This electron transfer results in the mutual formation of oxidized metal centers ($M^{\delta+}$) and reduced ceria atoms (Ce^{3+}), leading to changes in both their oxidation states. [43] These changes in oxidation state enhance the interactions of adsorbed molecules and the active centers on the metal, support, and interface, altogether improving catalytic performance.

Driven by the goal of reducing the use of costly precious metals, the strategy of placing isolated metal adatoms on oxide supports has recently gained considerable attention in the field of heterogeneous catalysis. Such systems, termed single atom catalysts (SACs), exhibit unique atomic and electronic structures, sometimes resulting in extraordinary catalytic activities. [44–50] Various metal oxides, including FeO_x, [45,51] Fe_2O_3, [52] Fe_3O_4, [53–55] TiO_2, [56–58] and CeO_2 [46,59–62] have been employed as supports for SACs. On the latter, several metal adatoms, such as Pt, Pd, Ag, and Cu have been successfully synthesized and tested for catalytic performance. [46, 55, 59–61, 63–65] For instance, Cu/CeO_2 is very effective in oxidation reactions, particularly CO oxidation, combining active Cu sites with the oxygen storage and release of ceria (oxygen buffer capacity). [46, 66, 67]

Jiang et al. synthesized single Cu atoms on CeO_2 clusters (2.4 nm in size) which were tested for CO_2 electroreduction. [68] Mosrati et al. reported high CO oxidation activity on single Cu sites supported on CeO_2-TiO_2 using *operando* techniques. [69] Building on previous studies of Cu/CeO_2 catalysts for CO and H_2 oxidation (PROX), [11,70,71] this work examines single Cu atoms supported on CeO_2 surfaces using density functional theory (DFT) calculations. We focus on the adsorption of molecular CO and H_2 and their subsequent oxidation reactions, as relevant for CO-PROX. In particular, the role of interfacial sites in the reactions, the redox activities, and formation of oxygen vacancies were evaluated. Our findings demonstrate that the oxidized single Cu site on CeO_2 serves as an active center for molecular adsorption of CO and H_2, thereby facilitating CO oxidation while H_2 remains intact. Overall, this underlines the catalytic potential of the Cu/CeO_2 single atom catalysts.

2 Computational details

Spin-polarized Kohn-Sham density functional theory (DFT) calculations were carried out using the Vienna ab initio simulation package (VASP) [72, 73] utilizing the projector-augmented-wave (PAW) method. [74,75] The Perdew-Burke-Ernzerhof (PBE) approximation to the generalized gradient approximation [76] was employed together with a Hubbard model using the Dudarev scheme, [77] where $U_{\rm eff} = 5.0$ eV was used for the localization of electrons in the $4f$-orbitals of Ce atoms. [37, 67] The occupation matrix control technique was applied to search for stable configurations of f-electrons at Ce atoms. [78] Initially, localized sites were individually screened for minimum energy at the upper and lower layers of CeO_2 surfaces with adsorbed Cu (Cu/CeO_2) by controlling the orbital occupation via the occupation matrix, subsequently, the resulting wavefunction was used as a starting guess for a SCF minimization without controlling the occupation matrix. The total energy was corrected by the D3 dispersion term proposed by Grimme et al. [79,80] Cutoff energy ($E_{\rm cut}$) for plane wave basis set for bulk (slab calculations) was 600 eV (450 eV) with a 6×6×6 (2×2×1) k-point sampling using a Monkhorst-Pack mesh. [81] The electronic self-consistency was considered converged, when the change of the total energy was smaller than 10^{-6} eV. All atoms were optimized until the forces acting ions were less than 20 meV/Å. Energy barriers were calculated using the nudged elastic band method (NEB). [82] The net atomic charge of individual atoms was analyzed using the Bader method. [83, 84]

The pristine low Miller index slabs, (111), (110), and (100) of CeO_2 with thicknesses of 11.03 Å, 9.68 Å, and 10.72 Å were cut from the optimized bulk CeO_2 and used for the adsorption of a single Cu atom. The non-polar CeO_2(111) surface was reported to be the most stable among the low-index surfaces, 0.91 J m^{-2}, the surface energy of (110) and (100) are described as substantially higher in energy, 1.56 J m^{-2} and 1.96 J m^{-2}, respectively. [85] Step edge morphologies have been reported on defective ceria surfaces (e.g., CeO_2(111)), [86–88] nevertheless; only pristine ceria surfaces were considered in the current study. A 12 Å vacuum gap and dipole moment correction were included in all surface slab models in the direction normal to the surfaces. [89] The binding energy of a single Cu atom was calculated by

$$E_b(hkl) = E_{\rm Cu/CeO_2} - (E_{\rm CeO_2} + E_{\rm Cu}) \quad (1)$$

where $E_{\rm Cu/CeO_2}$, $E_{\rm CeO_2}$, and $E_{\rm Cu}$ are total energies of $CeO_2(hkl)$ surface with an adsorbed Cu atom, bare CeO_2 surface, and isolated Cu atom in a gas phase. With this definition negative energies correspond to a favorable binding energy. In the same fashion, the molecular adsorption was calculated by

$$E_{ads}(X) = E_{X/\rm Cu/CeO_2} - (E_{\rm Cu/CeO_2} + E_X) \quad (2)$$

where the $E_{X/\rm Cu/CeO_2}$ is the total energy of a Cu/CeO_2 surface with an adsorbed molecule X and E_X describes a molecule X in a gas phase. Inversely, the desorption energy of molecule X was defined as the negative value of $E_{ads}(X)$. The oxygen vacancy formation energy at the surface was calculated as follows

$$E_{vac} = E_{\rm Cu/CeO_{2-x}} + \frac{1}{2}E_{\rm O_2} - E_{\rm Cu/CeO_2} \quad (3)$$

where $E_{\rm Cu/CeO_{2-x}}$ and $E_{\rm O_2}$ are total energies of a defective CeO_2 surface and a triplet oxygen in the gas phase, respectively. Reaction energies E_r and activation energies E_a were calculated by $E_r = E_{\rm pro} - E_{\rm react}$ and $E_a = E_{\rm TS} - E_{\rm react}$, respectively, where $E_{\rm react}$ is the total energy of a reactant state, $E_{\rm pro}$ is a total energy of a product state, and $E_{\rm TS}$ is a total energy at a transition state. Structure visualization and slab models were generated by VESTA [90] and ASE. [91]

3 Results and discussion

3.1 Geometry optimization of bulk CeO_2

Stoichiometric cerium oxide CeO_2 has a face-centered cubic structure within the $Fm\bar{3}m$ space group, the unit cell consisting of 4 cerium and 8 oxygen atoms (Fig. 1a). The cerium cations are coordinated by eight nearest-neighbor oxygen anions. Table S1 of the SI shows the lattice constant of bulk CeO_2 obtained by DFT with varying density functionals. In our study, we obtained a lattice constant, $a_0 = 5.46$ Å, which agrees well with the experimental value, 5.41 Å. [92, 93] An average Ce-O interatomic distance of 2.36 Å was determined. The average Bader charges of Ce and O atoms in a unit cell were +2.34 e^- and -1.17 e^-, presenting 4+ and 2- oxidation states for Ce and O, respectively. Surface slabs were then modeled from the optimized bulk CeO_2 structure.

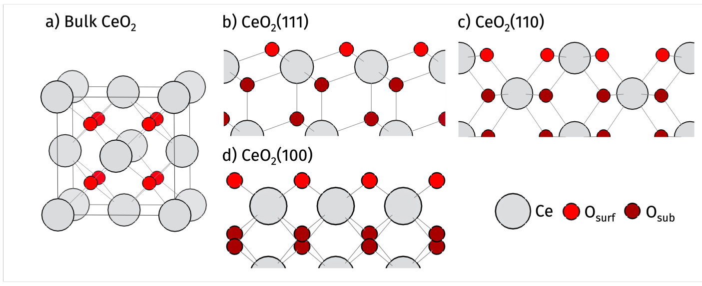

Figure 1: Cu/CeO_2 unit cell and its low-index surfaces: Side views of a) a bulk CeO_2 unit cell of cubic structure and its low Miller index surfaces, b) (111), c) (110), and d) (100). Cerium and oxygen atoms are color-coded in silver-white and red, respectively. In surface models, surface oxygen ($O_{\rm surf}$) is presented in red, while subsurface oxygen ($O_{\rm sub}$) is depicted in maroon.

3.2 Surface structures and adsorption of a single Cu atom

The low-index surfaces of CeO_2 show a stability in the order of (111)>(110)>(100), according to the reported surface energies. [23] The most stable non-polar (111) surface is terminated by three-fold coordinated oxygen atoms (Fig. 1b). The (110) and (100) surfaces are terminated by six-fold coordinated Ce and three-fold coordinated O, and two-fold coordinated O atoms (Fig. 1c,d). [23, 59]

Adsorption of a single Cu atom was modeled on stable sites of (111), (110), and (100) surfaces, analogous as reported by Qin et al. and Ji et al. [66, 67] We determined that low-index surfaces exhibit favorable binding energetics when a single Cu atom is attached, with its stability following the order (100)>(110)>(111) (Fig. 2 and Tab. 1). A Cu atom on the (100) surface has the highest binding energy of $E_b(100) = -4.62$ eV when it is bound on the bridging oxygen site, whereas the binding energy was less favorable on the other low-index surfaces, $E_b(110) = -3.84$ eV and $E_b(111) = -3.14$ eV, aligning reasonably well with previous studies. [67,94] Energy difference may arise from the binding environment of the adatom (e.g., nearest neighbors) on each surface (see Tab. 1). In addition, an adsorption energy of a single Cu atom on a larger cell, (4×4)-CeO_2(111), was calculated to be -2.94 eV (0.2 eV higher than (2×2)-CeO_2(111)). For Cu adatoms on pristine CeO_2(111), James et al. reported an experimental value of -2.32 eV at 100 K. [95] The calculated value in our study is substantially stronger, by 0.82 eV, as the calculations were carried out without accounting for zero point energy.

The adsorbed Cu atom is oxidized to Cu^+ by donating an electron to a surface Ce^{4+} atom, so that subsequently the cerium atom is reduced to Ce^{3+}, indicated by a change in charge, magnetic moment, and spin density of the Ce and Cu atoms, as shown in Fig. 2 and Tab. 1. The additional charge of ∼-0.5 e^- of Cu adatoms and magnetic moment of 0.96 μ_B obtained for localized Ce atoms are in good agreement with previous works. [33,67] The adsorbed Cu atoms are coordinated by three, two, and two nearest oxygen neighbors on (111), (110), and (100) surfaces, respectively.

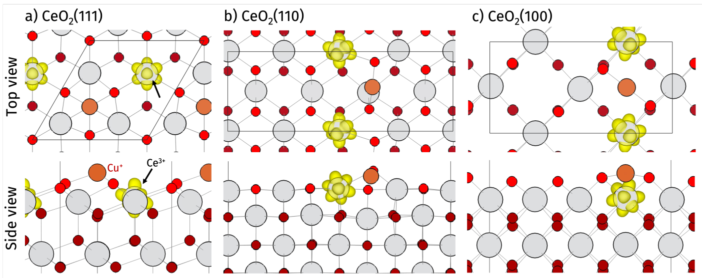

Figure 2: Top views (upper) and side views (lower) of optimized geometries of a single Cu atom (brown) adsorbed on truncated CeO_2: a) (111), b) (110), and c) (100) surfaces. Spin density isosurfaces are shown in yellow, presenting reduced Ce atoms (Ce^{3+} species).

To gain insight into electronic contributions, the projected electronic density of states (PDOS) of pristine CeO_2 and Cu adsorbed CeO_2 surfaces were calculated (Fig. 3). A wide gap of 2.29 eV between the valence-band and conduction-band edges was determined for the CeO_2(111) surface, consistent with the study of Piotrowski et al., ∼2.1 eV. [96] For CeO_2(110) and (100) surfaces, gaps of <2.0 eV were obtained. Upon adsorption of a Cu adatom, localized states of Ce($4f$) show up (between -0.75 and 0 eV), resulting from the localized charges introduced by the adsorbed Cu atom. At the Fermi level (shifted to 0 eV), the Cu($3d$) states are populated for Cu/CeO_2(111) and Cu/CeO_2(110) surfaces, while the localized Ce($4f$) state is predominant for the Cu/CeO_2(100) surface.

The Cu/CeO_2 surfaces were subsequently utilized to study CO and H_2 interactions occurring in surface reactions, as discussed below.

3.3 Molecular interaction of CO or H_2 with Cu/CeO_2

The interaction of molecular CO or H_2 was studied in terms of stability and oxidation processes on single Cu adatoms at

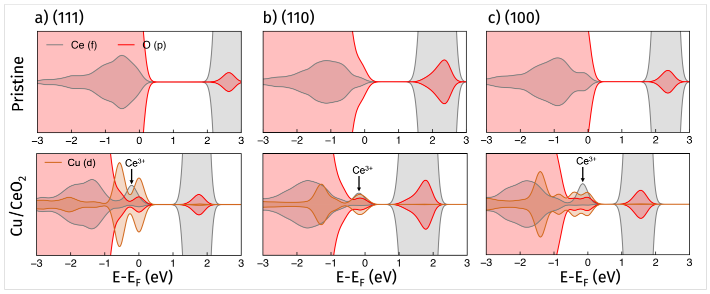

Figure 3: Projected electronic density of states (PDOS) of pristine (upper) and Cu-decorated (lower) ceria surfaces: a) CeO_2(111), b) CeO_2(110), and c) CeO_2(100) surfaces. PDOS of Ce(f), O(p), and Cu(d) are plotted in silver-white, red, and brown, respectively. A state of reduced cerium (Ce^{3+}) is indicated by a black arrow. The energy level is subtracted by Fermi energy.

CeO_2 surfaces. The interactions in the presence of CO or H_2 molecules at Cu sites on CeO_2 surfaces, including adsorption energies and atomic distances were examined.

3.3.1 CO adsorption:

CO chemisorbs (-1.39 eV) at a Cu atom on the CeO_2(111) surface, as illustrated in Fig. 4a. The distance between an atomic carbon of adsorbed CO and the Cu atom is 1.79 Å, and the C-O distance is slightly larger by 0.01 Å than calculated in the gas phase (1.14 Å). CO binds more strongly to the Cu site of Cu/CeO_2(111) than the Ce site of the pristine CeO_2(111) surface; for the latter with a reported unfavorable adsorption energy (ranging from -0.26 to 0.26 eV/CO) and a longer CO-surface distance (ranging from 2.86 to 2.88 Å). [97,98] According to our previous study, CO adsorption on a Cu^+ site of Cu/CeO_2(111) is more stable than on the Cu^+ site of the reduced CuO(111) surface, -1.39 eV *vs.* -1.29 eV. [11] On Cu/CeO_2(110) and Cu/CeO_2(100) surfaces, the adsorption energies of CO are -1.29 eV and -0.80 eV, respectively (Fig. 4b,c). The C-O bond length of adsorbed CO is 1.16 Å in both cases, marginally increased from the gas phase. The CO adsorption energy at Cu under the 2-fold coordination is similar to Cu/Fe_3O_4(001) [55] due to the similar binding environment of the Cu adatom and electronic structure. The Cu/CeO_2(111) surface provides the highest adsorption strength among the studied surfaces. The strong binding of CO on the Cu sites of Cu/CeO_2(111) and Cu/CeO_2(110) can be interpreted via the Cu(d) orbitals that are populated near the Fermi level, providing orbital interactions (back-donation) between the Cu atom and CO molecule (Fig. 3a,b). [99] Note that, upon CO adsorption on the Cu adatom, no lateral movement of the adatom occurs, as observed on Cu single crystals [100] or Au/CeO_2. [101] For Au/CeO_2(111), it was reported that Au adatom with adsorbed CO spontaneously diffused to the nearest site by relaxation. This shows the stability of single Cu adatoms on the CeO_2 surface during CO adsorption.

3.3.2 H_2 Oxidation:

In contrast to CO, H_2 shows weak interaction with the Cu sites of Cu/CeO_2(110) and Cu/CeO_2(100) surfaces (Fig. 4e,f), with negligible adsorption energies of -0.07 eV and -0.05 eV, respectively. These energies primarily arise from the con-

Table 1: Adsorption of a single Cu atom on CeO_2 (111), (110), and (100) surfaces: adsorption energies (E_{ads}), nearest neighbors of the adsorbed Cu atom, Bader charge difference of oxidized Cu, and magnetic moment of reduced Ce. Previously reported adsorption energies are in parentheses.

Surface	E_b (eV)	Cu NN	Δq_{Cu} (e^-)	M_{Ce} (μ_B)	Method
(111)	-3.14 (-2.83, -3.03) [67,94]	3	-0.65	0.96	
(110)	-3.84 (-3.81) [67]	2	-0.49	0.96	DFT+U
(100)	-4.62 (-4.45) [67]	2	-0.49	0.96	
(111)	(-2.94) [95]	-	-	-	Experiment

tribution of dispersion forces. The average H-Cu distance is 2.66 Å, with the H-H bond distance unchanged from the gas phase (0.75 Å), indicating a mere physisorption on (110) and (100) surfaces. In contrast, when H_2 adsorbs on the Cu site of $Cu/CeO_2(111)$ (Fig. 4d), the H-H bond slightly elongates to 0.82 Å, representing a 9% increase with respect to the gas phase, indicative of H_2 activation. The calculated adsorption energy is -0.37 eV, with a H-Cu distance of 1.68 Å. This finding aligns with a previous study by Righi et al., which demonstrated the activation of H_2 on noble metal single atoms (Cu, Ag, Au) deposited on the $CeO_2(111)$ surface. [102] In their study, H_2 adsorbed on the Cu site with an energy of -0.35 eV, and the H-H bond elongated to 0.84 Å.

H_2 activation is known as Kubas interaction, [103] which occurs when molecular H_2 in a side-on orientation interacts with transition metal centers. [104,105] This process involves the donation of σ-electrons from H_2 to the d-orbitals of the metal center, along with a simultaneous back-donation from the occupied d-orbitals of the metal center to the σ antibonding (σ^*) of H_2, resulting in elongation of the H-H bond.

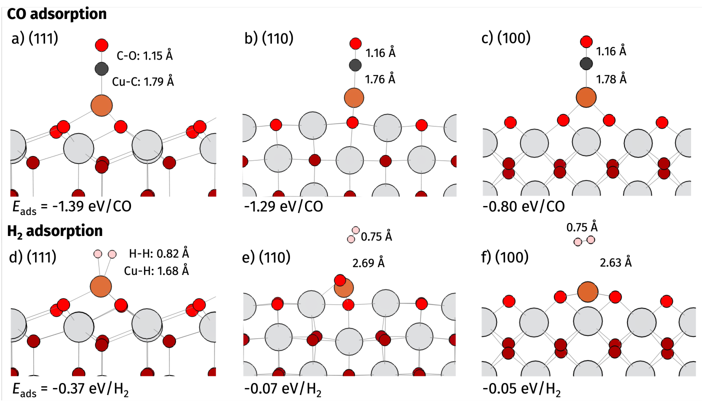

Figure 4: Side views of molecular adsorption on Cu/CeO_2 surfaces: a-c) CO and d-f) H_2 on Cu sites adsorbed on CeO_2 (111), (110), and (100) surfaces. Adsorption energies and atomic distances are shown. Carbon and hydrogen atoms are color-coded in dark-gray and pink, respectively.

In summary, the interaction of CO on a Cu site on CeO_2 surfaces represents chemical adsorption, with adsorption energies <-1.50 eV/CO observed for all studied surfaces except $Cu/CeO_2(100)$, which shows an energy of -0.80 eV/CO. Our study indicates that the presence of a single Cu atom on CeO_2 surface enhances the adsorption strength of a CO molecule, while on pristine CeO_2, only weak interaction occurs. [98,106] For H_2 adsorption, a weak interaction is observed, with adsorption energies ranging from -0.37 to -0.05 eV across the studied surfaces. Interestingly, a Kubas interaction occurs upon the adsorption on the Cu site of $Cu/CeO_2(111)$, resulting in non-dissociative elongation of the H_2 molecule. It is noteworthy that, compared to pure Cu NPs, CO adsorbs with energy ranging from -1.59 to -1.05 eV (depending on the size of NP), [107] while energies of -0.58 eV and -0.20 eV were reported for H_2 adsorption on a pure Cu_4 cluster [108] and Cu_{37} NP, [109] respectively.

Overall, our findings suggest that a single Cu atom adsorbed on the energetically most stable pristine $CeO_2(111)$ surface enhances the molecular CO adsorption strength, but only a weak interaction for H_2. These adsorption results serve as basis to rationalize various catalytic reactions, such as CO and H_2 oxidation, as well as the preferential oxidation of CO. [11] Below, $Cu/CeO_2(111)$ will be examined for such reaction studies, including the formation of oxygen vacancies (V_O).

3.4 Oxygen vacancy (V_O) formation on $Cu/CeO_2(111)$

Oxygen vacancies (V_O) play a vital role in various catalytic reactions on metal oxides by creating active sites and improving reaction activity. [11,110–112] In this study, we modeled two types of V_O sites: at the Cu/CeO_2 interface, where the oxygen atom is coordinated by four nearest neighbors (O_{4NN}), and at the site where the oxygen atom is coordinated by three nearest neighbors (O_{3NN}) (Fig. S1). Oxygen vacancy formation energies of 3.08 eV and 3.28 eV were obtained for V_{O3NN} and V_{O4NN}, respectively (see Tab. S2). The formation of V_O at O_{3NN} site is by 0.20 eV more stable than at the O_{4NN} site. After the formation of V_{O4NN}, a pseudo-linear Cu with surface oxygens is created. These energies are higher than those for the pristine $CeO_2(111)$ surface, which range from 2.00 to 2.50 eV per V_O using the same level of theory, PBE+U. [113]

The formation of a V_O results in two excess valence electrons that occupy the empty $4f$-orbitals of Ce atoms, leading to the reduction of Ce atoms, as visualized by the spin densities (Fig. S1b,c). In both cases (V_{O3NN} and V_{O4NN}), two Ce atoms are reduced, creating two additional Ce^{3+} species on the surface (in addition to one Ce atom reduced by the Cu adatom). For V_{O3NN}, one Ce^{3+} species is determined stable at the nearest neighbor sites to the oxygen vacancy, while the other is localized at a next-nearest neighbor in the subsurface. For V_{O4NN}, both Ce^{3+} species are located at the nearest neighbor sites to the vacancy.

Projected electronic density of states (PDOS) shows pronounced localized states of Ce(f) forming at the valence-band edges for both V_{O3NN} and V_{O4NN} (Fig. S2c,d). Compared to $Cu/CeO_2(111)$, these localized states are up-shifting to the Fermi levels, as indicated by pink arrows, resulting in a reduction in the bandgap between valence-band edge to conduction-band edge.

Our findings reveal that the presence of a Cu adatom increases the formation energy of V_O as compared to the pristine $CeO_2(111)$ surface. However, this higher energy suggests a more active surface for O_2 adsorption, facilitating the replenishment of surface vacancies and redox activities. [114] Additionally, the pronounced localized states of Ce(f) at the Fermi levels, resulting from V_O formation, are believed to enhance interactions with adsorbed molecules due to the presence of Ce^{3+} species. Nolan reported that Ce^{3+} promotes the interaction with NO_2. [115, 116] Regarding CO adsorption, both experimental and theoretical evidence suggest that CO adsorbs weakly on the ceria sites, even in the presence of Ce^{3+} species. [117] This confirms that noble metal adatoms, like Cu, are beneficial for promoting CO adsorption on ceria surfaces.

The presence of oxygen vacancies (V_O) on the Cu/CeO_2 surface, particularly at the Cu/CeO_2 interface, is crucial for governing oxidation processes, especially via Mars-van Krevelen mechanism in heterogeneous oxide catalysts. The role of V_O in facilitating the oxidation reactions of CO and H_2 is described below.

3.5 Oxidation reactions of CO or H_2 on $Cu/CeO_2(111)$

3.5.1 CO oxidation:

The oxidation of CO to CO_2 was studied following a Mars-van Krevelen mechanism, a common pathway in heterogenous oxide catalysis, [11,12,118,119] including CeO_2. [120–125] Initially, we examined CO oxidation on the $Cu/CeO_2(111)$ surface (Fig. 5). A gas phase CO molecule easily adsorbs on a Cu site with a reaction energy $E_r(\mathbf{1} \rightarrow \mathbf{2}) = -1.39$ eV. The interaction between the adsorbed CO and lattice oxygen, forming a bent CO_2^- intermediate, [67,87] is endothermic with $E_r(\mathbf{2} \rightarrow \mathbf{4}) = 0.63$ eV and a reaction barrier $E_a(\mathbf{3})$ of 0.64 eV. The calculated barrier is similar to that determined in a previous DFT study (0.51 eV). [67] The C-O bond distance and O-C-O angle of bent CO_2 are reduced by 2.5% and 34.2%, respectively, compared to the gas phase. The stability of this intermediate was confirmed as no imaginary modes were found in the frequency calculations. In a similar fashion, a CO_2 molecule may be activated at a vacancy site V_O.

After the formation of a bent CO_2^- intermediate, it desorbs into the gas phase, generating an oxygen vacancy (V_O) at the Cu-CeO_2 interface, with a reaction energy $E_r(\mathbf{4} \rightarrow \mathbf{5}) = 0.59$ eV. As described above, V_O creates two additional Ce^{3+} species. Subsequently, an O_2 replenishes the V_O site in a downhill process, $E_r(\mathbf{5} \rightarrow \mathbf{6}) = -3.03$ eV. The adsorbed O_2^* is a singlet O_2^- species with a O-O bond elongation of 21.1% from the gas phase and, simultaneously, two Ce^{3+} are re-oxidized back to Ce^{4+} states. This shows that the oxygen molecule is spontaneously activated by V_O as observed for various oxide catalysts. [11, 111, 126, 127] The second CO oxidation then proceeds exothermically without a barrier on the $\frac{1}{2}O_2^*$ site with $E_r(\mathbf{6} \rightarrow \mathbf{7a}) = -3.66$ eV, while being less exothermic on the Cu site, $E_r(\mathbf{6} \rightarrow \mathbf{7b}) = -0.91$ eV. Finally, the desorption of CO_2 from step (**7a**) proceeds with a desorption energy of 0.42 eV, completing the catalytic cycle (**8**).

3.5.2 H_2 oxidation:

The oxidation pathway of H_2 to H_2O was examined (Fig. 6). Firstly, an H_2 molecule adsorbs on a single Cu site with a small adsorption energy $E_r(\mathbf{1} \rightarrow \mathbf{2}) = -0.37$ eV, causing

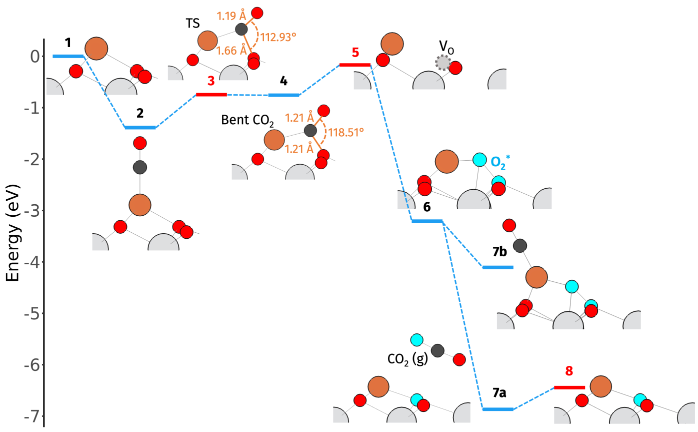

Figure 5: Reaction pathway of CO oxidation. Starting from the bare $Cu/CeO_2(111)$ surface (**1**), CO first adsorbs on a Cu site (**2**) and forms with lattice O into a bent CO_2^- intermediate (**4**) by crossing a transition state TS (**3**). A vacancy site V_O is generated after the desorption of CO_2 into the gas phase (**5**). A gas phase O_2 (cyan spheres) then replenishes the V_O (**6**). A second CO adsorbs on $\frac{1}{2}O_2^*$ (**7a**) or on Cu (**7b**), the former directly forms CO_2 and then desorbs as gas phase CO_2 (**8**). Desorption energy and transition states (TS) are labeled by red bars/numbers.

the H-H bond to elongate from its gas phase distance, as previously described. The H atom then interacts with a lattice O to form a stable OH species, with a reaction energy $E_r(\mathbf{2} \rightarrow \mathbf{4}) = -0.42$ eV and a barrier $E_a(\mathbf{3})$ of 0.52 eV. Compared to the CO oxidation barrier (0.64 eV), the barrier for OH formation is lower by 0.12 eV, suggesting that OH species may occur during the oxidation in mixed-gas environments (e.g., preferential CO oxidation conditions).

To complete H_2 oxidation, the adsorbed H reacts with an OH species to form H_2O (step **4** $\rightarrow$ **6**). This reaction is endothermic with $E_r(\mathbf{4} \rightarrow \mathbf{6}) = 0.41$ eV and a high barrier $E_a(\mathbf{5}) = 1.43$ eV. The desorption of the formed H_2O into the gas phase requires an energy of 0.93 eV (**7**). Thus, H_2O formation and desorption are more challenging compared to CO_2.

The formation of H_2O creates a V_O that is favorable to be filled by molecular O_2 (step **7** $\rightarrow$ **8**) as described in **Section** 3.5.1. A second H_2 molecule then adsorbs energetically on a Cu site with $E_r(\mathbf{8} \rightarrow \mathbf{9}) = -0.22$ eV, causing a slight H-H bond elongation. Once again, an H atom proceeds to react with a $\frac{1}{2}O_2^*$ species to form an OH species with $E_r(\mathbf{9} \rightarrow \mathbf{11}) = -1.27$ eV and a barrier of 0.14 eV. The resulting OH species is attached on a Cu site adjacent to the adsorbed H (**11**). Finally, the adsorbed H exothermically reacts with OH to form H_2O with $E_r(\mathbf{11} \rightarrow \mathbf{13}) = -1.81$ eV and a low barrier $E_a(\mathbf{12}) = 0.10$ eV, and the formed H_2O then desorbs into a gas phase with $E_r(\mathbf{13} \rightarrow \mathbf{14}) = 0.74$ eV.

Overall, the rate-determining step of CO oxidation on the $Cu/CeO_2(111)$ surface is the formation of the bent CO_2^- intermediate (a CO spillover to the oxide support) with a reaction barrier of 0.64 eV (step **3**). In contrast, the rate-determining step for H_2 oxidation is the reaction between the adsorbed H and OH to form H_2O, which has a significantly higher barrier of 1.43 eV (step **5**). These findings highlight that CO oxidation proceeds more favorably on this surface than H_2 oxidation due to its lower rate-limiting step. Additionally, it is notable that OH species may form during H_2 oxidation,

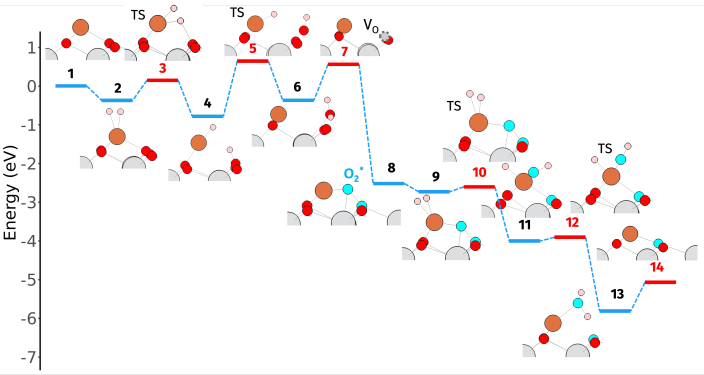

Figure 6: Reaction pathway of H_2 oxidation. Starting from the bare $Cu/CeO_2(111)$ surface (**1**), H_2 first adsorbs on a Cu site (**2**) and $\frac{1}{2}H_2$ forms with lattice O into a OH species (**4**) with a barrier (**3**), leaving Cu-H. Then, the adsorbed H atom on Cu site forms with the OH species into H_2O (**6**) by crossing a high barrier (**5**) and then desorbs into a H_2O(g), creating a vacancy site V_O (**7**). A gas phase O_2 (cyan spheres) fills exothermically at the V_O (**8**). A second H_2 adsorbs on a Cu site (**9**), crossing a barrier (**10**), to forms a second OH species that attached on the Cu site (**11**). By crossing a low barrier (**12**), the adsorbed H interacts with an OH to form a second H_2O (**13**) and subsequently desorbs into a gas phase H_2O(g), completing a cycle (**14**). Desorption energy and transition states (TS) are labeled by red bars/numbers.

which could influence the catalytic reactions, [128, 129] particularly in mixed-gas environments.

Conclusions

In this study, we investigated the adsorption characteristics and catalytic activity of single Cu atoms on different CeO_2 surfaces, focusing on the oxidation of CO and H_2 and the role of oxygen vacancies. Our findings demonstrate that low-index CeO_2 surfaces may stabilize Cu adatoms, following a stability trend of (100)>(110)>(111). The Cu adatoms donate charge to a Ce, reducing Ce^{4+} to Ce^{3+} and oxidizing Cu^0 to Cu^+. This enhances molecular adsorption energetics at the Cu site compared to the pristine CeO_2.

CO adsorption is notably strong at the Cu site on the $CeO_2(111)$ surface due to favorable interactions between the CO and Cu(d) orbitals, while H_2 adsorption is weaker, involving a Kubas-type interaction that modestly activates the H-H bond. The Mars-van Krevelen type mechanism was applied to model CO and H_2 oxidation, where an oxygen vacancy V_O formation plays a key role. For CO oxidation, interaction between CO and lattice O forms a bent CO_2^- intermediate that subsequently desorbs as a gas phase CO_2. For H_2 oxidation, it involves H_2 dissociation into Cu-H and OH species, which then combine to form H_2O. Following the formation of both CO_2 and H_2O, V_O are created, which facilitates subsequent O_2 adsorption and then creates highly active O species, promoting the catalytic cycle. In the case of H_2 oxidation, the pathway is energetically less favorable due to a higher rate-determining barrier compared to the CO oxidation pathway.

In summary, single Cu atoms on CeO_2 significantly enhance CO adsorption and promote CO oxidation, while also offering some interaction with H_2, although less strongly. The findings highlight that Cu/CeO_2 provides a stable, active surface for CO oxidation, with potential applications in heterogeneous catalysis, particularly for reactions involving CO.

Conflict of interest statement

The authors declare no conflict of interest.

Data access statement

DFT data supporting the research is available in the ioChem-DB database.

Ethics statement

The research includes no studies on human subjects, human data or tissue, or animals.

Acknowledgements

This research was funded by the Austrian Science Fund (FWF) [10.55776/F81] (SFB TACO, P08). We are grateful for generous computing resources at the Vienna Scientific Cluster (VSC). P.L.T acknowledges fruitful discussions with Lyudmila V. Moskaleva on ceria modeling.

References

[1] Lele Peng, Pan Xiong, Lu Ma, Yifei Yuan, Yue Zhu, Dahong Chen, Xiangyi Luo, Jun Lu, Khalil Amine, and Guihua Yu. Holey two-dimensional transition metal oxide nanosheets for efficient energy storage. *Nature Communications*, 8(1):15139, April 2017.

[2] Parthiban Pazhamalai, Vignesh Krishnan, Mohamed Sadiq Mohamed Saleem, Sang-Jae Kim, and Hye-Won Seo. Investigating composite electrode materials of metal oxides for advanced energy storage applications. *Nano Convergence*, 11(1):30, July 2024.

[3] Yu Liu, Xiaomin Xu, Zongping Shao, and San Ping Jiang. Metal-organic frameworks derived porous carbon, metal oxides and metal sulfides-based compounds for supercapacitors application. *Energy Storage Materials*, 26:1–22, April 2020.

[4] Alexander K. Opitz, Andreas Nenning, Christoph Rameshan, Markus Kubicek, Thomas Götsch, Raoul Blume, Michael Hävecker, Axel Knop-Gericke, Günther Rupprechter, Bernhard Klötzer, and Jürgen Fleig. Surface Chemistry of Perovskite-Type Electrodes During High Temperature CO_2 Electrolysis Investigated by *Operando* Photoelectron Spectroscopy. *ACS Applied Materials & Interfaces*, 9(41):35847–35860, October 2017.

[5] Alexander K. Opitz, Andreas Nenning, Christoph Rameshan, Raffael Rameshan, Raoul Blume, Michael Hävecker, Axel Knop-Gericke, Günther Rupprechter, Jürgen Fleig, and Bernhard Klötzer. Enhancing Electrochemical Water-Splitting Kinetics by Polarization-Driven Formation of Near-Surface Iron(0): An In Situ XPS Study on Perovskite-Type Electrodes. *Angewandte*

Chemie International Edition, 54(9):2628–2632, February 2015.

[6] Yu-Feng Sun, Shao-Bo Liu, Fan-Li Meng, Jin-Yun Liu, Zhen Jin, Ling-Tao Kong, and Jin-Huai Liu. Metal Oxide Nanostructures and Their Gas Sensing Properties: A Review. *Sensors*, 12(3):2610–2631, February 2012.

[7] Alexey A. Tomchenko, Gregory P. Harmer, Brent T. Marquis, and John W. Allen. Semiconducting metal oxide sensor array for the selective detection of combustion gases. *Sensors and Actuators B: Chemical*, 93(1-3):126–134, August 2003.

[8] Sofian M. Kanan, Oussama M. El-Kadri, Imad A. Abu-Yousef, and Marsha C. Kanan. Semiconducting Metal Oxide Based Sensors for Selective Gas Pollutant Detection. *Sensors*, 9(10):8158–8196, October 2009.

[9] Qaisar Maqbool, Nevzat Yigit, Michael Stöger-Pollach, Maria Letizia Ruello, Francesca Tittarelli, and Günther Rupprechter. *Operando* monitoring of a room temperature nanocomposite methanol sensor. *Catalysis Science & Technology*, 13(3):624–636, 2023.

[10] Jingxia Yang, Shuaishuai Peng, Yunjing Shi, Shuyi Ma, Huihui Ding, Günther Rupprechter, and Jinjie Wang. Fast visual evaluation of the catalytic activity of CeO_2: Simple colorimetric assay using 3,3,5,5-tetramethylbenzidine as indicator. *Journal of Catalysis*, 389:71–77, September 2020.

[11] Parinya Tangpakonsab, Alexander Genest, Jingxia Yang, Ali Meral, Bingjie Zou, Nevzat Yigit, Sabine Schwarz, and Günther Rupprechter. Kinetic and Computational Studies of CO Oxidation and PROX on Cu/CeO2 Nanospheres. *Topics in Catalysis*, 66(15-16):1129–1142, September 2023.

[12] Liliana Lukashuk, Nevzat Yigit, Raffael Rameshan, Elisabeth Kolar, Detre Teschner, Michael Hävecker, Axel Knop-Gericke, Robert Schlögl, Karin Föttinger, and Günther Rupprechter. Operando Insights into CO Oxidation on Cobalt Oxide Catalysts by NAP-XPS, FTIR, and XRD. *ACS Catalysis*, 8(9):8630–8641, September 2018.

[13] Nevzat Yigit, Alexander Genest, Schamil Terloev, Jury Möller, and Günther Rupprechter. Active sites and deactivation of room temperature CO oxidation on Co_3O_4 catalysts: combined experimental and computational investigations. *Journal of Physics: Condensed Matter*, 34(35):354001, August 2022.

[14] Yvan J. O. Asencios, Nevzat Yigit, Thomas Wicht, Michael Stöger-Pollach, Alessandra F. Lucrédio, Francielle C. F. Marcos, Elisabete M. Assaf, and Günther Rupprechter. Partial Oxidation of Bio-methane over Nickel Supported on $MgO–ZrO_2$ Solid Solutions. *Topics in Catalysis*, 66(19-20):1539–1552, November 2023.

[15] Jingxia Yang, Nevzat Yigit, Jury Möller, and Günther Rupprechter. Co_3O_4 CeO_2 Nanocomposites for Low-Temperature CO Oxidation. *Chemistry – A European Journal*, 27(68):16947–16955, December 2021.

[16] Günther Rupprechter. Operando Surface Spectroscopy and Microscopy during Catalytic Reactions: From Clusters via Nanoparticles to Meso-Scale Aggregates. *Small*, 17(27):2004289, July 2021.

[17] Jacques Védrine. Heterogeneous Catalysis on Metal Oxides. *Catalysts*, 7(11):341, November 2017.

[18] Lichen Liu and Avelino Corma. Metal Catalysts for Heterogeneous Catalysis: From Single Atoms to Nanoclusters and Nanoparticles. *Chemical Reviews*, 118(10):4981–5079, May 2018.

[19] Asha Gupta, U. V. Waghmare, and M. S. Hegde. Correlation of Oxygen Storage Capacity and Structural Distortion in Transition-Metal-, Noble-Metal-, and Rare-Earth-Ion-Substituted CeO_2 from First Principles Calculation. *Chemistry of Materials*, 22(18):5184–5198, September 2010.

[20] Joachim Paier, Christopher Penschke, and Joachim Sauer. Oxygen Defects and Surface Chemistry of Ceria: Quantum Chemical Studies Compared to Experiment. *Chemical Reviews*, 113(6):3949–3985, June 2013.

[21] Katarzyna A. Michalow-Mauke, Ye Lu, Kazimierz Kowalski, Thomas Graule, Maarten Nachtegaal, Oliver Kröcher, and Davide Ferri. Flame-Made WO_3/CeO_x - TiO_2 Catalysts for Selective Catalytic Reduction of NO $_x$ by NH_3. *ACS Catalysis*, 5(10):5657–5672, October 2015.

[22] Luca Artiglia, Fabrizio Orlando, Kanak Roy, René Kopelent, Olga Safonova, Maarten Nachtegaal, Thomas Huthwelker, and Jeroen A. Van Bokhoven. Introducing Time Resolution to Detect Ce^{3+} Catalytically Active Sites at the Pt/CeO_2 Interface through Ambient Pressure X-ray Photoelectron Spectroscopy. *The Journal of Physical Chemistry Letters*, 8(1):102–108, January 2017.

[23] M. Verónica Ganduglia-Pirovano, Alexander Hofmann, and Joachim Sauer. Oxygen vacancies in transition metal and rare earth oxides: Current state of understanding and remaining challenges. *Surface Science Reports*, 62(6):219–270, June 2007.

[24] Zongyuan Liu, David C. Grinter, Pablo G. Lustemberg, Thuy-Duong Nguyen-Phan, Yinghui Zhou, Si Luo, Iradwikanari Waluyo, Ethan J. Crumlin, Dario J. Stacchiola, Jing Zhou, Javier Carrasco, H. Fabio Busnengo, M. Verónica Ganduglia-Pirovano, Sanjaya D. Senanayake, and José A. Rodriguez. Dry Reforming of Methane on a Highly-Active Ni-CeO_2 Catalyst: Effects of Metal-Support Interactions on CH Bond Breaking. *Angewandte Chemie International Edition*, 55(26):7455–7459, June 2016.

[25] Jingxia Yang, Huihui Ding, Jinjie Wang, Nevzat Yigit, Jingli Xu, Günther Rupprechter, Min Zhang, and Zhiquan Li. Energy-Guided Shape Control Towards Highly Active CeO_2. *Topics in Catalysis*, 63(19-20):1743–1753, December 2020.

[26] Huihui Ding, Jingxia Yang, Shuyi Ma, Nevzat Yigit, Jingli Xu, Günther Rupprechter, and JinJie Wang.

Large Dimensional CeO_2 Nanoflakes by Microwave-Assisted Synthesis: Lamellar Nano-Channels and Surface Oxygen Vacancies Promote Catalytic Activity. *ChemCatChem*, 10(18):4100–4108, September 2018.

[27] Na Ta, Jingyue (Jimmy) Liu, Santhosh Chenna, Peter A. Crozier, Yong Li, Aling Chen, and Wenjie Shen. Stabilized Gold Nanoparticles on Ceria Nanorods by Strong Interfacial Anchoring. *Journal of the American Chemical Society*, 134(51):20585–20588, December 2012.

[28] Yang-Gang Wang, Donghai Mei, Vassiliki-Alexandra Glezakou, Jun Li, and Roger Rousseau. Dynamic formation of single-atom catalytic active sites on ceria-supported gold nanoparticles. *Nature Communications*, 6(1):6511, March 2015.

[29] Junjie Shi, Hailian Li, Alexander Genest, Weixuan Zhao, Pengfei Qi, Tao Wang, and Günther Rupprechter. High-performance water gas shift induced by asymmetric oxygen vacancies: Gold clusters supported by ceria-praseodymia mixed oxides. *Applied Catalysis B: Environmental*, 301:120789, February 2022.

[30] Noelia Barrabés, Jon Ostolaza, Sarah Reindl, Martin Mähr, Florian Schrenk, Hedda Drexler, Christoph Rameshan, Wojciech Olszewski, and Günther Rupprechter. Doped metal clusters as bimetallic AuCo nanocatalysts: insights into structural dynamics and correlation with catalytic activity by *in situ* spectroscopy. *Faraday Discussions*, 242:94–105, 2023.

[31] Vera Truttmann, Hedda Drexler, Michael Stöger-Pollach, Tokuhisa Kawawaki, Yuichi Negishi, Noelia Barrabés, and Günther Rupprechter. CeO_2 Supported Gold Nanocluster Catalysts for CO Oxidation: Surface Evolution Influenced by the Ligand Shell. *ChemCatChem*, 14(14):e202200322, July 2022.

[32] Stephan Pollitt, Vera Truttmann, Thomas Haunold, Clara Garcia, Wojciech Olszewski, Jordi Llorca, Noelia Barrabés, and Günther Rupprechter. The Dynamic Structure of $Au_{38}(SR)_{24}$ Nanoclusters Supported on CeO_2 upon Pretreatment and CO Oxidation. *ACS Catalysis*, 10(11):6144–6148, June 2020.

[33] Rui Zhang, Arunabhiram Chutia, Alexey A. Sokol, David Chadwick, and C. Richard A. Catlow. A computational investigation of the adsorption of small copper clusters on the $CeO_2(110)$ surface. *Physical Chemistry Chemical Physics*, 23(35):19329–19342, 2021.

[34] Arunabhiram Chutia, Emma K. Gibson, Matthew R. Farrow, Peter P. Wells, David O. Scanlon, Nikolaos Dimitratos, David J. Willock, and C. Richard A. Catlow. The adsorption of Cu on the CeO_2 (110) surface. *Physical Chemistry Chemical Physics*, 19(40):27191–27203, 2017.

[35] Wei-Wei Wang, Wen-Zhu Yu, Pei-Pei Du, Hui Xu, Zhao Jin, Rui Si, Chao Ma, Shuo Shi, Chun-Jiang Jia, and Chun-Hua Yan. Crystal Plane Effect of Ceria on Supported Copper Oxide Cluster Catalyst for CO Oxidation: Importance of Metal–Support Interaction. *ACS Catalysis*, 7(2):1313–1329, February 2017.

[36] Changjun Zhang, Angelos Michaelides, and Stephen J. Jenkins. Theory of gold on ceria. *Phys. Chem. Chem. Phys.*, 13(1):22–33, 2011.

[37] Weihua Ji, Xin Chen, Qiang Li, Kun Lin, Jinxia Deng, and Xianran Xing. Insights into CO Oxidation in Cu/CeO_2 Catalysts: O_2 Activation at the Dual-Interfacial Sites. *European Journal of Inorganic Chemistry*, 26(10):e202200656, April 2023.

[38] Yanmin Liu, Dongsen Mao, Jun Yu, Xiaoming Guo, and Zhen Ma. Low-temperature CO oxidation on CuO-CeO_2 catalyst prepared by facile one-step solvothermal synthesis: Improved activity and moisture resistance via optimizing the activation temperature. *Fuel*, 332:126196, January 2023.

[39] José A. Hernández, Sergio A. Gómez, T. A. Zepeda, Juan C. Fierro-González, and Gustavo A. Fuentes. Insight into the Deactivation of Au/CeO_2 Catalysts Studied by In Situ Spectroscopy during the CO-PROX Reaction. *ACS Catalysis*, 5(7):4003–4012, July 2015.

[40] Marc Ziemba, M. Verónica Ganduglia-Pirovano, and Christian Hess. Insight into the mechanism of the water–gas shift reaction over Au/CeO_2 catalysts using combined *operando* spectroscopies. *Faraday Discussions*, 229:232–250, 2021.

[41] Yi-Chong Chen and Gui-Chang Wang. Structure Sensitivity of the Water–Gas Shift Reaction over Cu/CeO_2: A Combination of DFT, MF-MKM, and kMC. *The Journal of Physical Chemistry C*, 128(24):9926–9939, June 2024.

[42] Denis Leybo, Ubong J. Etim, Matteo Monai, Simon R. Bare, Ziyi Zhong, and Charlotte Vogt. Metal–support interactions in metal oxide-supported atomic, cluster, and nanoparticle catalysis. *Chemical Society Reviews*, 53(21):10450–10490, 2024.

[43] Oleksii Bezkrovnyi, Albert Bruix, Dominik Blaumeiser, Lesia Piliai, Simon Schötz, Tanja Bauer, Ivan Khalakhan, Tomáš Skála, Peter Matvija, Piotr Kraszkiewicz, Mirosława Pawlyta, Mykhailo Vorokhta, Iva Matolínová, Jörg Libuda, Konstantin M. Neyman, and Leszek Kpiński. Metal–Support Interaction and Charge Distribution in Ceria-Supported Au Particles Exposed to CO. *Chemistry of Materials*, 34(17):7916–7936, September 2022.

[44] Gareth S. Parkinson. Single-Atom Catalysis: How Structure Influences Catalytic Performance. *Catalysis Letters*, 149(5):1137–1146, May 2019.

[45] Botao Qiao, Aiqin Wang, Xiaofeng Yang, Lawrence F. Allard, Zheng Jiang, Yitao Cui, Jingyue Liu, Jun Li, and Tao Zhang. Single-atom catalysis of CO oxidation using Pt_1/FeO_x. *Nature Chemistry*, 3(8):634–641, August 2011.

[46] Zheng Chen, Zhangyun Liu, and Xin Xu. Dynamic evolution of the active center driven by hemilabile coordination in Cu/CeO_2 single-atom catalyst. *Nature Communications*, 14(1):2512, May 2023.

[47] Aiqin Wang, Jun Li, and Tao Zhang. Heterogeneous single-atom catalysis. *Nature Reviews Chemistry*, 2(6):65–81, May 2018.

[48] Selina K. Kaiser, Zupeng Chen, Dario Faust Akl, Sharon Mitchell, and Javier Pérez-Ramírez. Single-Atom Catalysts across the Periodic Table. *Chemical Reviews*, 120(21):11703–11809, November 2020.

[49] Florian Kraushofer and Gareth S. Parkinson. Single-Atom Catalysis: Insights from Model Systems. *Chemical Reviews*, 122(18):14911–14939, September 2022.

[50] Niancai Cheng, Lei Zhang, Kieran Doyle-Davis, and Xueliang Sun. Single-Atom Catalysts: From Design to Application. *Electrochemical Energy Reviews*, 2(4):539–573, December 2019.

[51] Jinxia Liang, Qi Yu, Xiaofeng Yang, Tao Zhang, and Jun Li. A systematic theoretical study on FeO_x-supported single-atom catalysts: M_1/FeO_x for CO oxidation. *Nano Research*, 11(3):1599–1611, March 2018.

[52] Ali Rafsanjani-Abbasi, Florian Buchner, Faith J. Lewis, Lena Puntscher, Florian Kraushofer, Panukorn Sombut, Moritz Eder, Jiří Pavelec, Erik Rheinfrank, Giada Franceschi, Viktor Birschitzky, Michele Riva, Cesare Franchini, Michael Schmid, Ulrike Diebold, Matthias Meier, Georg K. H. Madsen, and Gareth S. Parkinson. Digging Its Own Site: Linear Coordination Stabilizes a Pt_1/Fe_2O_3 Single-Atom Catalyst. *ACS Nano*, 18(39):26920–26927, October 2024.

[53] Roland Bliem, Jessi E. S. Van Der Hoeven, Jan Hulva, Jiri Pavelec, Oscar Gamba, Petra E. De Jongh, Michael Schmid, Peter Blaha, Ulrike Diebold, and Gareth S. Parkinson. Dual role of CO in the stability of subnano Pt clusters at the Fe_3O_4(001) surface. *Proceedings of the National Academy of Sciences*, 113(32):8921–8926, August 2016.

[54] Gareth S. Parkinson, Zbynek Novotny, Giacomo Argentero, Michael Schmid, Jiří Pavelec, Rukan Kosak, Peter Blaha, and Ulrike Diebold. Carbon monoxide-induced adatom sintering in a Pd–Fe_3O_4 model catalyst. *Nature Materials*, 12(8):724–728, August 2013.

[55] Jan Hulva, Matthias Meier, Roland Bliem, Zdenek Jakub, Florian Kraushofer, Michael Schmid, Ulrike Diebold, Cesare Franchini, and Gareth S. Parkinson. Unraveling CO adsorption on model single-atom catalysts. *Science*, 371(6527):375–379, January 2021.

[56] Ho Viet Thang, Gianfranco Pacchioni, Leo DeRita, and Phillip Christopher. Nature of stable single atom Pt catalysts dispersed on anatase TiO_2. *Journal of Catalysis*, 367:104–114, November 2018.

[57] Leo DeRita, Sheng Dai, Kimberly Lopez-Zepeda, Nicholas Pham, George W. Graham, Xiaoqing Pan, and Phillip Christopher. Catalyst Architecture for Stable Single Atom Dispersion Enables Site-Specific Spectroscopic and Reactivity Measurements of CO Adsorbed to Pt Atoms, Oxidized Pt Clusters, and Metallic Pt Clusters on TiO_2. *Journal of the American Chemical Society*, 139(40):14150–14165, October 2017.

[58] Wenjie Zang, Jaeha Lee, Peter Tieu, Xingxu Yan, George W. Graham, Ich C. Tran, Peikui Wang, Phillip Christopher, and Xiaoqing Pan. Distribution of Pt single atom coordination environments on anatase TiO_2 supports controls reactivity. *Nature Communications*, 15(1):998, February 2024.

[59] Nathan Daelman, Marçal Capdevila-Cortada, and Núria López. Dynamic charge and oxidation state of Pt/CeO_2 single-atom catalysts. *Nature Materials*, 18(11):1215–1221, November 2019.

[60] Valery Muravev, Giulia Spezzati, Ya-Qiong Su, Alexander Parastaev, Fu-Kuo Chiang, Alessandro Longo, Carlos Escudero, Nikolay Kosinov, and Emiel J. M. Hensen. Interface dynamics of Pd–CeO_2 single-atom catalysts during CO oxidation. *Nature Catalysis*, 4(6):469–478, June 2021.

[61] Zhiqiang Wang, Xiaomei Zhou, Gehui Wang, Qing Tong, Haiqin Wan, and Lin Dong. High-Performance Ir_1/CeO_2 Single-Atom Catalyst for the Oxidation of Toluene. *Inorganic Chemistry*, 63(16):7241–7254, April 2024.

[62] Bing Han, Tianbo Li, Junying Zhang, Chaobin Zeng, Hiroaki Matsumoto, Yang Su, Botao Qiao, and Tao Zhang. A highly active Rh_1/CeO_2 single-atom catalyst for low-temperature CO oxidation. *Chemical Communications*, 56(36):4870–4873, 2020.

[63] Filip Dvořák, Matteo Farnesi Camellone, Andrii Tovt, Nguyen-Dung Tran, Fabio R. Negreiros, Mykhailo Vorokhta, Tomáš Skála, Iva Matolínová, Josef Mysliveček, Vladimír Matolín, and Stefano Fabris. Creating single-atom Pt-ceria catalysts by surface step decoration. *Nature Communications*, 7(1):10801, February 2016.

[64] Yubo Liang, Cailing Wu, Songjie Meng, Zhansheng Lu, Runyao Zhao, Huiyong Wang, Zhimin Liu, and Jianji Wang. Ag Single Atoms Anchored on CeO_2 with Interfacial Oxygen Vacancies for Efficient CO_2 Electroreduction. *ACS Applied Materials & Interfaces*, 15(25):30262–30271, June 2023.

[65] Yongli Shen, Kangjuan Yin, and Zihui Xiao. Theoretical insight into the single-atom catalytic mechanism of CeO_2-supported Ag catalysts in CO oxidation. *Physical Chemistry Chemical Physics*, 21(36):20346–20353, 2019.

[66] Lan Qin, Yun-Qi Cui, Tao-Li Deng, Fu-Hua Wei, and Xiang-Fei Zhang. Highly stable and Active Cu_1/CeO_2 Single-Atom Catalyst for CO Oxidation: A DFT Study. *ChemPhysChem*, 19(24):3346–3349, December 2018.

[67] Weihua Ji, Na Wang, Xin Chen, Qiang Li, Kun Lin, Jinxia Deng, Jun Chen, and Xianran Xing. Effects of Subsurface Oxide on Cu_1/CeO_2 Single-Atom Catalysts for CO Oxidation: A Theoretical Investigation. *Inorganic Chemistry*, 61(26):10006–10014, July 2022.

[68] Yawen Jiang, Keke Mao, Jiawei Li, Delong Duan, Jiayi Li, Xinyu Wang, Yuan Zhong, Chao Zhang, Hengjie Liu, Wanbing Gong, Ran Long, and Yujie Xiong. Pushing the Performance Limit of Cu/CeO_2 Catalyst in CO_2

Electroreduction: A Cluster Model Study for Loading Single Atoms. *ACS Nano*, 17(3):2620–2628, February 2023.

[69] Jawaher Mosrati, Ali M. Abdel-Mageed, Thanh Huyen Vuong, Reni Grauke, Stephan Bartling, Nils Rockstroh, Hanan Atia, Udo Armbruster, Sebastian Wohlrab, Jabor Rabeah, and Angelika Brückner. Tiny Species with Big Impact: High Activity of Cu Single Atoms on CeO_2 –TiO_2 Deciphered by *Operando* Spectroscopy. *ACS Catalysis*, 11(17):10933–10949, September 2021.

[70] Nicolas Bion, Florence Epron, Máximo Moreno, Fernando Mariño, and Daniel Duprez. Preferential Oxidation of Carbon Monoxide in the Presence of Hydrogen (PROX) over Noble Metals and Transition Metal Oxides: Advantages and Drawbacks. *Topics in Catalysis*, 51(1-4):76–88, December 2008.

[71] Aline Rodrigues Miranda Cruz, Elisabete Moreira Assaf, Janaina Fernandes Gomes, and José Mansur Assaf. Active copper species of co-precipitated copper-ceria catalysts in the CO-PROX reaction: An in situ XANES and DRIFTS study. *Catalysis Today*, 381:42–49, December 2021.

[72] G. Kresse and J. Furthmüller. Efficiency of ab-initio total energy calculations for metals and semiconductors using a plane-wave basis set. *Computational Materials Science*, 6(1):15–50, July 1996.

[73] G. Kresse and J. Furthmüller. Efficient iterative schemes for *ab initio* total-energy calculations using a plane-wave basis set. *Physical Review B*, 54(16):11169–11186, October 1996.

[74] P. E. Blöchl. Projector augmented-wave method. *Physical Review B*, 50(24):17953–17979, December 1994.

[75] G. Kresse and D. Joubert. From ultrasoft pseudopotentials to the projector augmented-wave method. *Physical Review B*, 59(3):1758–1775, January 1999.

[76] John P. Perdew, Kieron Burke, and Matthias Ernzerhof. Generalized Gradient Approximation Made Simple. *Physical Review Letters*, 77(18):3865–3868, October 1996.

[77] S. L. Dudarev, G. A. Botton, S. Y. Savrasov, C. J. Humphreys, and A. P. Sutton. Electron-energy-loss spectra and the structural stability of nickel oxide: An LSDA+U study. *Physical Review B*, 57(3):1505–1509, January 1998.

[78] Jeremy P. Allen and Graeme W. Watson. Occupation matrix control of d- and f-electron localisations using DFT + U. *Phys. Chem. Chem. Phys.*, 16(39):21016–21031, 2014.

[79] Stefan Grimme, Jens Antony, Stephan Ehrlich, and Helge Krieg. A consistent and accurate *ab initio* parametrization of density functional dispersion correction (DFT-D) for the 94 elements H-Pu. *The Journal of Chemical Physics*, 132(15):154104, April 2010.

[80] Stefan Grimme, Stephan Ehrlich, and Lars Goerigk. Effect of the damping function in dispersion corrected density functional theory. *Journal of Computational Chemistry*, 32(7):1456–1465, May 2011.

[81] Hendrik J. Monkhorst and James D. Pack. Special points for Brillouin-zone integrations. *Physical Review B*, 13(12):5188–5192, June 1976.

[82] Graeme Henkelman and Hannes Jónsson. Improved tangent estimate in the nudged elastic band method for finding minimum energy paths and saddle points. *The Journal of Chemical Physics*, 113(22):9978–9985, December 2000.

[83] Graeme Henkelman, Andri Arnaldsson, and Hannes Jónsson. A fast and robust algorithm for Bader decomposition of charge density. *Computational Materials Science*, 36(3):354–360, June 2006.

[84] W Tang, E Sanville, and G Henkelman. A grid-based Bader analysis algorithm without lattice bias. *Journal of Physics: Condensed Matter*, 21(8):084204, February 2009.

[85] Zhao Liu, Charles C. Sorrell, Pramod Koshy, and Judy N. Hart. DFT Study of Methanol Adsorption on Defect-Free CeO_2 Low-Index Surfaces. *ChemPhysChem*, 20(16):2074–2081, August 2019.

[86] Niklas Nilius, Sergey M. Kozlov, Jan-Frederick Jerratsch, Martin Baron, Xiang Shao, Francesc Viñes, Shamil Shaikhutdinov, Konstantin M. Neyman, and Hans-Joachim Freund. Formation of One-Dimensional Electronic States along the Step Edges of CeO_2(111). *ACS Nano*, 6(2):1126–1133, February 2012.

[87] De-Ren Chu, Zhi-Qiang Wang, and Xue-Qing Gong. Theoretical insights into CO oxidation activities on CeO2(111) steps. *Surface Science*, 722:122096, August 2022.

[88] María M. Branda, Christoph Loschen, Konstantin M. Neyman, and Francesc Illas. Atomic and Electronic Structure of Cerium Oxide Stepped Model Surfaces. *The Journal of Physical Chemistry C*, 112(45):17643–17651, November 2008.

[89] Jörg Neugebauer and Matthias Scheffler. Adsorbate-substrate and adsorbate-adsorbate interactions of Na and K adlayers on Al(111). *Physical Review B*, 46(24):16067–16080, December 1992.

[90] Koichi Momma and Fujio Izumi. *VESTA 3* for three-dimensional visualization of crystal, volumetric and morphology data. *Journal of Applied Crystallography*, 44(6):1272–1276, December 2011.

[91] Ask Hjorth Larsen, Jens Jørgen Mortensen, Jakob Blomqvist, Ivano E Castelli, Rune Christensen, Marcin Dułak, Jesper Friis, Michael N Groves, Bjørk Hammer, Cory Hargus, Eric D Hermes, Paul C Jennings, Peter Bjerre Jensen, James Kermode, John R Kitchin, Esben Leonhard Kolsbjerg, Joseph Kubal, Kristen Kaasbjerg, Steen Lysgaard, Jón Bergmann Maronsson, Tristan Maxson, Thomas Olsen, Lars Pastewka, Andrew Peterson, Carsten Rostgaard, Jakob Schiøtz, Ole Schütt, Mikkel Strange, Kristian S Thygesen, Tejs Vegge, Lasse Vilhelmsen, Michael Walter, Zhenhua Zeng, and Karsten W Jacobsen. The atomic simulation environment—a Python library for working with atoms. *Journal of Physics: Condensed Matter*, 29(27):273002, July 2017.

[92] Steven J. Duclos, Yogesh K. Vohra, Arthur L. Ruoff, A. Jayaraman, and G. P. Espinosa. High-pressure x-ray diffraction study of CeO_2 to 70 GPa and pressure-induced phase transformation from the fluorite structure. *Physical Review B*, 38(11):7755–7758, October 1988.

[93] L. Gerward and J. Staun Olsen. Powder diffraction analysis of cerium dioxide at high pressure. *Powder Diffraction*, 8(2):127–129, June 1993.

[94] Lucie Szabová, Matteo Farnesi Camellone, Min Huang, Vladimír Matolín, and Stefano Fabris. Thermodynamic, electronic and structural properties of Cu/CeO_2 surfaces and interfaces from first-principles DFT+U calculations. *The Journal of Chemical Physics*, 133(23):234705, December 2010.

[95] Trevor E. James, Stephanie L. Hemmingson, and Charles T. Campbell. Energy of Supported Metal Catalysts: From Single Atoms to Large Metal Nanoparticles. *ACS Catalysis*, 5(10):5673–5678, October 2015.

[96] Maurício J. Piotrowski, Polina Tereshchuk, and Juarez L. F. Da Silva. Theoretical Investigation of Small Transition-Metal Clusters Supported on the CeO_2(111) Surface. *The Journal of Physical Chemistry C*, 118(37):21438–21446, September 2014.

[97] Min Huang and Stefano Fabris. CO Adsorption and Oxidation on Ceria Surfaces from DFT+U Calculations. *The Journal of Physical Chemistry C*, 112(23):8643–8648, June 2008.

[98] Michael Nolan and Graeme W. Watson. The Surface Dependence of CO Adsorption on Ceria. *The Journal of Physical Chemistry B*, 110(33):16600–16606, August 2006.

[99] R.R. Ford. Carbon Monoxide Adsorption on the Transition Metals. In *Advances in Catalysis*, volume 21, pages 51–150. Elsevier, 1970.

[100] Matteo Roiaz, Laura Falivene, Christoph Rameshan, Luigi Cavallo, Sergey M. Kozlov, and Günther Rupprechter. Roughening of Copper (100) at Elevated CO Pressure: Cu Adatom and Cluster Formation Enable CO Dissociation. *The Journal of Physical Chemistry C*, 123(13):8112–8121, April 2019.

[101] Matteo Farnesi Camellone and Stefano Fabris. Reaction Mechanisms for the CO Oxidation on Au/CeO_2 Catalysts: Activity of Substitutional Au^{3+}/Au^{+} Cations and Deactivation of Supported Au^{+} Adatoms. *Journal of the American Chemical Society*, 131(30):10473–10483, August 2009.

[102] Giulia Righi, Rita Magri, and Annabella Selloni. H_2 Dissociation on Noble Metal Single Atom Catalysts Adsorbed on and Doped into CeO_2(111). *The Journal of Physical Chemistry C*, 123(15):9875–9883, April 2019.

[103] Gregory J. Kubas. Molecular hydrogen complexes: coordination of a .sigma. bond to transition metals. *Accounts of Chemical Research*, 21(3):120–128, March 1988.

[104] Ashley L. Sutton, James I. Mardel, and Matthew R. Hill. Metal-Organic Frameworks (MOFs) As Hydrogen Storage Materials At Near-Ambient Temperature. *Chemistry – A European Journal*, 30(44):e202400717, August 2024.

[105] Simona Müllerová, Michal Malček, Lukas Bucinsky, and Maria Natália Dias Soeiro Cordeiro. Exploring hydrogen binding and activation on transition metal-modified circumcoronene. *Carbon Letters*, 34(5):1495–1506, June 2024.

[106] Ya-Ling Song, Li-Li Yin, Jie Zhang, P. Hu, Xue-Qing Gong, and Guanzhong Lu. A DFT+U study of CO oxidation at CeO_2(110) and (111) surfaces with oxygen vacancies. *Surface Science*, 618:140–147, December 2013.

[107] Wilke Dononelli and Thorsten Klüner. CO adsorption and oxygen activation on group 11 nanoparticles – a combined DFT and high level CCSD(T) study about size effects and activation processes. *Faraday Discussions*, 208:105–121, 2018.

[108] Luis E. Gálvez-González, Julio A. Alonso, Lauro Oliver Paz-Borbón, and Alvaro Posada-Amarillas. H_2 Adsorption on $Cu_{4\text{-x}}M_x$ (M = Au, Pt; x = 0–4) Clusters: Similarities and Differences As Predicted by Density Functional Theory. *The Journal of Physical Chemistry C*, 123(51):30768–30780, December 2019.

[109] Thomas Wicht, Alexander Genest, Lidia E. Chinchilla, Thomas Haunold, Andreas Steiger-Thirsfeld, Michael Stöger-Pollach, José J. Calvino, and Günther Rupprechter. Role of Interfacial Hydrogen in Ethylene Hydrogenation on Graphite-Supported Ag, Au, and Cu Catalysts. *ACS Catalysis*, pages 16905–16919, November 2024.

[110] Qihang Zhao, Liangjie Fu, Denghui Jiang, Jing Ouyang, Yuehua Hu, Huaming Yang, and Yunfei Xi. Nanoclay-modulated oxygen vacancies of metal oxide. *Communications Chemistry*, 2(1):11, January 2019.

[111] Ji Yang, Siyu Hu, Yarong Fang, Son Hoang, Li Li, Weiwei Yang, Zhenfeng Liang, Jian Wu, Jinpeng Hu, Wen Xiao, Chuanqi Pan, Zhu Luo, Jun Ding, Lizhi Zhang, and Yanbing Guo. Oxygen Vacancy Promoted O_2 Activation over Perovskite Oxide for Low-Temperature CO Oxidation. *ACS Catalysis*, 9(11):9751–9763, November 2019.

[112] Wenbin Jiang, Hongyi Loh, Beverly Qian Ling Low, Houjuan Zhu, Jingxiang Low, Jerry Zhi Xiong Heng, Karen Yuanting Tang, Zibiao Li, Xian Jun Loh, Enyi Ye, and Yujie Xiong. Role of oxygen vacancy in metal oxides for photocatalytic CO_2 reduction. *Applied Catalysis B: Environmental*, 321:122079, February 2023.

[113] M. Verónica Ganduglia-Pirovano, Juarez L. F. Da Silva, and Joachim Sauer. Density-Functional Calculations of the Structure of Near-Surface Oxygen Vacancies and Electron Localization on CeO_2(111). *Physical Review Letters*, 102(2):026101, January 2009.

[114] Arantxa Davó-Quiñonero, Esther Bailón-García, Sergio López-Rodríguez, Jerónimo Juan-Juan, Dolores

Lozano-Castelló, Max García-Melchor, Facundo C. Herrera, Eric Pellegrin, Carlos Escudero, and Agustín Bueno-López. Insights into the Oxygen Vacancy Filling Mechanism in CuO/CeO_2 Catalysts: A Key Step Toward High Selectivity in Preferential CO Oxidation. *ACS Catalysis*, 10(11):6532–6545, June 2020.

[115] Siqi Shi, Yuanhao Tang, Chuying Ouyang, Lixia Cui, Xiaogui Xin, Peijuan Li, Weiwei Zhou, Hua Zhang, Minsheng Lei, and Liquan Chen. O-vacancy and surface on CeO_2: A first-principles study. *Journal of Physics and Chemistry of Solids*, 71(5):788–796, May 2010.

[116] Michael Nolan. Formation of Ce^{3+} at the cerium dioxide (110) surface by doping. *Chemical Physics Letters*, 492(1-3):115–118, May 2010.

[117] Kumudu Mudiyanselage, Hyun You Kim, Sanjaya D. Senanayake, Ashleigh E. Baber, Ping Liu, and Dario Stacchiola. Probing adsorption sites for CO on ceria. *Physical Chemistry Chemical Physics*, 15(38):15856, 2013.

[118] M. Lewandowski, I.M.N. Groot, S. Shaikhutdinov, and H.-J. Freund. Scanning tunneling microscopy evidence for the Mars-van Krevelen type mechanism of low temperature CO oxidation on an FeO(111) film on Pt(111). *Catalysis Today*, 181(1):52–55, February 2012.

[119] P Broqvist. A DFT Study on CO Oxidation over Co_3O_4. *Journal of Catalysis*, 210(1):198–206, August 2002.

[120] Hyun You Kim and Graeme Henkelman. CO Oxidation at the Interface of Au Nanoclusters and the Stepped-CeO_2(111) Surface by the Mars–van Krevelen Mechanism. *The Journal of Physical Chemistry Letters*, 4(1):216–221, January 2013.

[121] Yukiko Hosono, Hikaru Saito, Takuma Higo, Kosuke Watanabe, Kazuharu Ito, Hideaki Tsuneki, Shun Maeda, Kunihide Hashimoto, and Yasushi Sekine. Co–CeO_2 Interaction Induces the Mars–van Krevelen Mechanism in Dehydrogenation of Ethane. *The Journal of Physical Chemistry C*, 125(21):11411–11418, June 2021.

[122] Yanru Wang, Jiamin Ma, Xiuyi Wang, Zheshan Zhang, Jiahan Zhao, Jie Yan, Yaping Du, Hongbo Zhang, and Ding Ma. Complete CO Oxidation by O_2 and H_2O over Pt–CeO_2/MgO Following Langmuir–Hinshelwood and Mars–van Krevelen Mechanisms, Respectively. *ACS Catalysis*, 11(19):11820–11830, October 2021.

[123] Tian Tang, Lyumeng Ye, Yanrong Chen, Jingyu Xue, Xiaoqiang Shen, Jinfei Chen, Fiona Hammond Quarcoo, Vladislav Rac, Vesna Rakić, Xinbao Li, and Xuesen Du. Diving into the interface-mediated Mars-van Krevelen (MvK) characteristic of CuO_x-supported CeO_2 catalysts. *Applied Catalysis B: Environmental*, 342:123368, March 2024.

[124] Chunlei Wang, Xiang-Kui Gu, Huan Yan, Yue Lin, Junjie Li, Dandan Liu, Wei-Xue Li, and Junling Lu. Water-Mediated Mars–Van Krevelen Mechanism for CO Oxidation on Ceria-Supported Single-Atom Pt_1 Catalyst. *ACS Catalysis*, 7(1):887–891, January 2017.

[125] Kenichi Koizumi, Katsuyuki Nobusada, and Mauro Boero. The absence of a gap state and enhancement of the Mars–van Krevelen reaction on oxygen defective Cu/CeO_2 surfaces. *Physical Chemistry Chemical Physics*, 18(30):20708–20712, 2016.

[126] Igor Sokolović, Michele Reticcioli, Martin Čalkovský, Margareta Wagner, Michael Schmid, Cesare Franchini, Ulrike Diebold, and Martin Setvín. Resolving the adsorption of molecular O_2 on the rutile TiO_2(110) surface by noncontact atomic force microscopy. *Proceedings of the National Academy of Sciences*, 117(26):14827–14837, June 2020.

[127] Yaguang Zhu, Jianyu Wang, Shyam Bharatkumar Patel, Chaoran Li, Ashley R. Head, Jorge Anibal Boscoboinik, and Guangwen Zhou. Tuning the surface reactivity of oxides by peroxide species. *Proceedings of the National Academy of Sciences*, 120(13):e2215189120, March 2023.

[128] Dongqing Wang, Rongtan Li, Xiaoyuan Sun, Le Lin, Kun Li, Rankun Zhang, Rentao Mu, and Qiang Fu. Hydroxide Structure-Dependent OH Promotion Mechanism over a Hydroxylated CoO_x/Pt(111) Catalyst toward CO Oxidation. *ACS Catalysis*, 14(7):5147–5155, April 2024.

[129] Lina Cao, Wei Liu, Qiquan Luo, Ruoting Yin, Bing Wang, Jonas Weissenrieder, Markus Soldemo, Huan Yan, Yue Lin, Zhihu Sun, Chao Ma, Wenhua Zhang, Si Chen, Hengwei Wang, Qiaoqiao Guan, Tao Yao, Shiqiang Wei, Jinlong Yang, and Junling Lu. Atomically dispersed iron hydroxide anchored on Pt for preferential oxidation of CO in H_2. *Nature*, 565(7741):631–635, January 2019.